ELSEVIER

Nuclear Instruments and Methods in Physics Research A 459 (2001) 365–376

NUCLEAR INSTRUMENTS & METHODS IN PHYSICS RESEARCH Section A

www.elsevier.nl/locate/nima

Neutron tomographic fissile assay in spent fuel using the lead slowing down time spectrometer

Yong-Deok Lee[a], R.C. Block[b,*], R.E. Slovacek[b], D.R. Harris[b], N.M. Abdurrahman[c]

[a]*Korea Atomic Energy Research Institute, Nuclear Data Evaluation Lab., P.O. Box 105, Yousung, Taejon 305-600, South Korea*
[b]*Rensselaer Polytechnic Institute, Department of Environmental and Energy Engineering, Gaerttner Linac Laboratory, Troy, NY 12180-3590, USA*
[c]*The University of Texas at Austin, Department of Mechanical Engineering, Nuclear Engineering Teaching Laboratory, Austin, TX 78712, USA*

Received 18 March 1999; received in revised form 25 July 2000; accepted 21 August 2000

Abstract

A tomographical fissile assay technique for light water reactor spent fuels was developed based on the lead slowing down time spectrometer (LSDTS). The Monte Carlo method was used for system performance and for simulation of the sensitivity of detection of fissile materials using neutron emission tomography. A typical spent PWR fuel element was simulated and the spatial and mass sensitivity of the fissile components were investigated. From these studies, the LSDTS system is shown to be a very sensitive device for analyzing the spatial distribution of total fissile materials of a spent fuel assembly in a properly selected assay neutron energy range. This method is also applicable to nuclear waste assay.

PACS: 28.20.Gd; 28.41.Kw; 29.25.Dz; 29.40. − n

Keywords: Tomography; Lead slowing down time spectrometer; Detectors; Linac; Resolution; Fissile assay

1. Introduction

The non-destructive assay of the fissile isotopic content of spent fuel is important for nuclear safeguards, nuclear safety, nuclear fuel management, and the economic use of fissile materials [1–3]. To overcome the intense γ and neutron background associated with spent fuel, especially fuel which has not been allowed to decay over many years, the lead slowing down time spectrometer (LSDTS) assay method was developed at Rensselaer Polytechnic Institute (RPI) to determine simultaneously each fissile component in spent fuel. Earlier measurements at the RPI Gaerttner LINAC Laboratory demonstrated the effectiveness of using a LSDTS for simultaneous assay of each fissile component in a simulated fuel assembly [4]. A LSDTS was subsequently designed for the practical assay of spent LWR fuel, a design which led to a reduced capital cost and to a system which could be used effectively for spent fuel assay at a nuclear power plant, a reprocessing facility, or a nuclear repository site [5]. As discussed in Refs. [4,5]

* Corresponding author. Tel.: + 1-518-276-6406; fax: + 1-518-276-4007.
E-mail addresses: ydlee@nanum.kaeri.re.kr (Y.-D. Lee), blockr@rpi.edu, slovar@rpi.edu (R.C. Block), naeem@mail.utexas.edu (N.M. Abdurrahman).

0168-9002/01/$ - see front matter
PII: S0168-9002(00)01016-0

the intensity of the fission signal produced by the neutron source greatly exceeds the fission background from spent fuel such that this background is not a problem for an LSDTS system.

Spent fuel assemblies generally have radial and axial asymmetry of burnup due to the neutron flux distribution in a reactor core. Therefore, effects caused by internal material inhomogeneity must be considered to get more accurate non-destructive assay results. The objective of this work was to find a proper LSDTS system condition for spatial fissile assay and to examine how sensitively spatial fissile assay could be reconstructed in a simulated fuel assembly by measuring the emitted prompt fast fission neutrons.

A practical device for assaying spent fuel should have the following characteristics:

(i) Be able to assay spent fuel in the presence of γ radiation levels up to $\sim 10^5$ rad/h.
(ii) Be insensitive to the presence of fertile materials (^{238}U, ^{232}Th, ^{240}Pu, etc.).
(iii) Be insensitive to background neutrons emanating from the spent fuel (from processes like spontaneous fission from transactinides or (α, n) reactions in oxygen of the fuel).
(iv) Assay each fissile isotope (rather than just 'average fissile material').
(v) Be able to provide a spatial assay which can be used to determine assymetries of burnup and/or possible diversion of fissile material.

An LSDTS system provides all five of these characteristics [4]. The use of a one-section low-energy electron accelerator to produce an intense pulse of source of photoneutrons can significantly reduce the cost of a practical LSDTS [5–8]. The photoneutron reaction produces an evaporation spectrum, i.e. the boiling off of neutrons from the excited target nucleus. The evaporation spectrum is given, in the calculations to be described, by

$$N_s(E)\,dE = (E/T^2)\exp[-(E/T)]\,dE \quad (1)$$

where E is the neutron energy and T is the photonuclear target temperature, both in units of MeV. The spectrum of fission neutrons produced inside the spent fuel is represented as a Watt spectrum [9]. The Watt spectrum is given by

$$N_f(E) = C\exp[-(E/a)]\sinh(bE)^{1/2} \quad (2)$$

where, for example, a and b are taken to be 0.988 MeV and 2.249 MeV^{-1} for ^{235}U [9].

A broad range of interrogation neutron energies results within the lead spectrometer. The interrogation energy range between 1 keV and 0.1 eV is very sensitive to the fissile material and it provides good energy resolution in the fission signatures coming from the fissile isotopes [4]. The threshold fission detectors used here have a low sensitivity to decay radiations emanating from the spent fuel. During assay the lead acts as a shield of intense γ-rays, thus enabling very active fuel elements to be assayed, even in the necessarily dry LSDTS.

2. Neutron emission tomography

2.1. Lead slowing down time spectrometer

The LSDTS has been developed with the purpose of assaying the fissile material content of irradiated fuel elements efficiently, effectively and practically. The general description of the assay method is an optimized cylindrical lead pile driven by an intense pulsed neutron source, as shown in Fig. 1. The spent fuel assembly is inserted into the center of the lead cylinder. The LSDTS uses an electron linear accelerator and a photoneutron target[1] for producing interrogation source neutrons by $(e,\gamma)(\gamma, n)$ reactions. These interrogating neutrons induce fission in the fissile (^{235}U, ^{239}Pu and ^{241}Pu) materials during the interrogation time interval but not significantly in the fertile materials (^{232}Th, ^{238}U) during this interval. By using threshold fission detectors (^{238}U) placed close to the spent fuel, the occurrence of fission events in the spent fuel can be detected and registered in a slowing down time analyzer.

The analysis of the detected prompt fission neutrons by the assay detectors involves the characteristic fission from the fissile materials and simultaneously determines the content of each of the fissile materials. For this study a PWR fuel

[1] The electron linear accelerator at Rensselaer Polytechnic Institute (RPI) is 60 MeV in energy and uses 1 kW beam power for assay measurements.

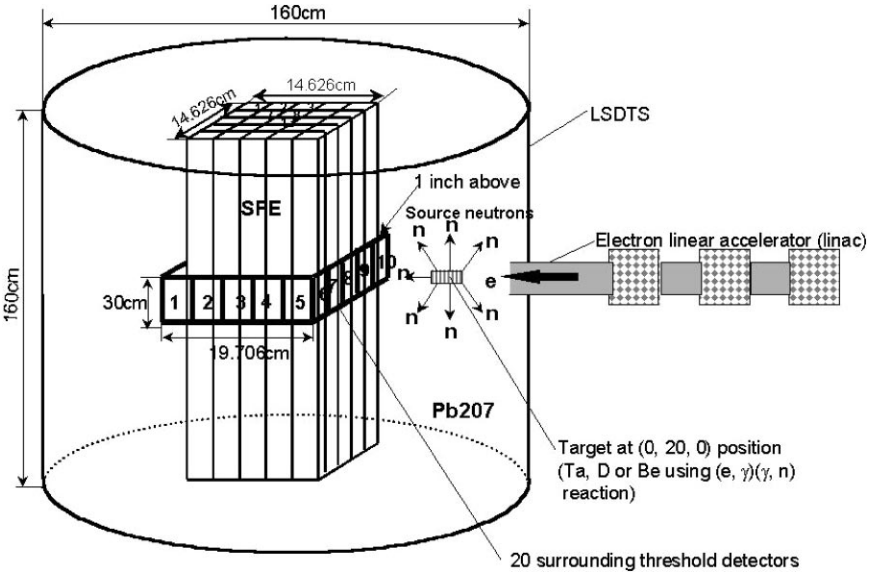

Fig. 1. LSDTS for tomographical fissile assay of spent fuel.

Table 1
Material composition of the spent fuel used in the simulation: ORIGEN2 code was used (PWR, 33,000 MWd/MTU)

Material	Grams (g) in a metric ton
^{16}O	1.34×10^{5}
^{90}Zr	1.17×10^{5}
^{91}Zr	2.62×10^{4}
^{92}Zr	4.04×10^{4}
^{93}Zr	7.18×10^{2}
^{94}Zr	4.19×10^{4}
^{96}Zr	7.54×10^{3}
^{235}U	7.93×10^{3}
^{238}U	9.44×10^{5}
^{239}Pu	5.03×10^{3}
^{241}Pu	1.16×10^{3}

element was selected as representative of a typical fuel element. Table 1 shows the material composition selected in the simulation of a PWR spent fuel element (SFE), using the ORIGEN2 code [10] with a specific burnup of 33,000 MWd/MTU with 3.5 wt% initial enrichment.

Fig. 1 shows the major area of the LSDTS device with the threshold detectors for spent fuel fissile assay. The lead assembly is a 160 cm right circular cylinder with the spent fuel elements placed in the center. The SFE is surrounded by 30 cm long threshold fission detectors (^{238}U) placed 2.54 cm from the fuel surface. The pulsed neutron source is located inside the lead assembly outside of the spent fuel region.

Fig. 2 shows a midplane representation of the SFE and detectors inside the LSDTS. For the purpose of this analysis, the SFE is divided into a 5×5 matrix of cells ($c=1,\cdots,25$) with the pulsed neutron source placed outside of cell number 15. The ^{238}U fission neutron detectors are represented by 20 cells ($m=1,\cdots,20$) placed in the lead and separated from the surface of the SFE by 2.54 cm of lead.

The Monte Carlo code MCNP [9] was used to simulate the distribution of the interrogation neutrons and the prompt fission neutrons in the fuel cells, and to determine the detector response to prompt fission neutrons in each cell. The spatial prompt fission neutron distribution inside the SFE is calculated by

$$\phi_{f_{\mathrm{cell}}}=\sum_{\substack{^{235}\mathrm{U}\\ ^{239}\mathrm{Pu}\\ ^{241}\mathrm{Pu}}}\left[\int_{t1}^{t2}\int_{0}^{\infty}\int_{V_{\mathrm{cell}}}\nu(E)\sigma_{\mathrm{f}}(E)\phi(r,E,t)\,\mathrm{d}r\,\mathrm{d}E\,\mathrm{d}t\right]_{i} \tag{3}$$

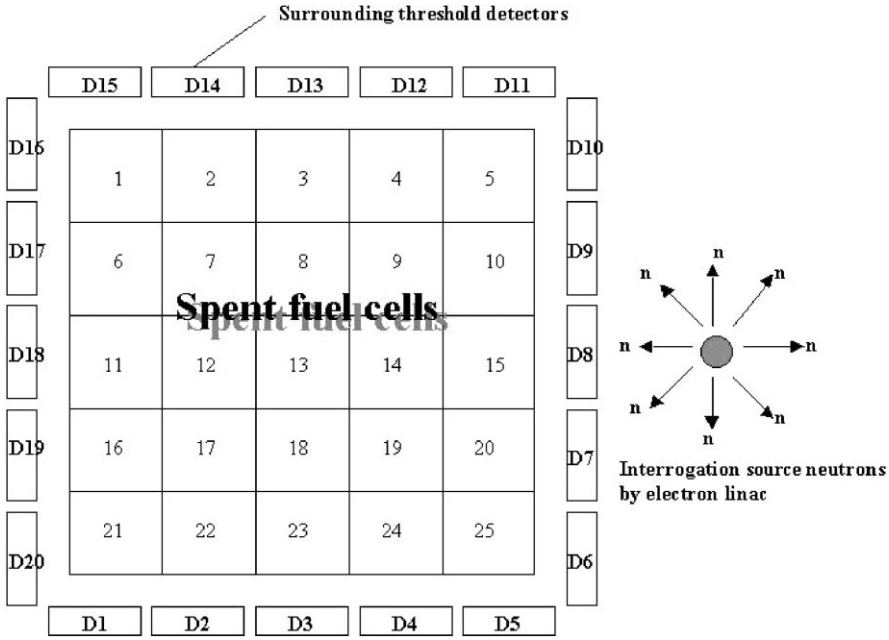

Fig. 2. Schematic view of the fuel cells and the threshold detectors.

where the fast prompt fission neutron flux is integrated over the total slowing down time range with the spatial dependence and with the contribution from all fissile materials in the spent fuel [5]. The contribution of the fertile materials in the slowing-down time range is negligible. The neutron interrogation flux arriving at the fuel cell is $\phi(r, E, t)$, $\sigma_f(E)$ is the fission cross-section at energy E, and $\nu(E)$ is the number of fission neutrons released per fission. The results of the Monte Carlo calculation are shown in Table 2 for the normalized interrogation neutron and induced prompt fission neutron distributions in the 25 fuel cells of the spent fuel assembly; 50,000 neutron case histories were used for this calculation. The upper number is the cell number, the middle number is the normalized interrogation neutron fluence in the cell, and the bottom number is the normalized fission neutron fluence in the cell. As can be seen in Fig. 2 the neutron source is placed closest to cell number 15 and this is evident in Table 2 in the peaking of the interrogation and fission fluences in the cells on the side of the SFE nearest the neutron source ($c = 5, 10, 15, 20$ and 25).

The detector sensitivity, or response, to the prompt fission neutrons from all the spent fuel cells

Table 2
Normalized interrogation neutron and induced prompt fission neutron fluences inside the spent fuel assembly. In each cell ($c = 1, \ldots, 25$) the middle numbers are the interrogation neutron fluence and the bottom numbers are the fission neutron fluence (in units of 10^{-5} per cm^2)

1	2	3	4	5
18.13	17.55	18.31	19.50	22.40
1.261	1.225	1.200	1.344	1.492
6	7	8	9	10
17.10	16.05	16.51	17.95	20.90
1.125	1.021	1.060	1.061	1.300
11	12	13	14	15
16.18	15.87	15.95	17.04	20.37
1.195	1.045	0.956	1.067	1.253
16	17	18	19	20
16.30	16.09	16.16	17.55	20.17
1.087	0.983	0.975	1.084	1.239
21	22	23	24	25
17.75	17.24	17.85	19.02	21.75
1.079	1.061	1.147	1.208	1.292

was also determined by the MCNP code by the surface crossing tally

$$\int_{S_{\mathrm{det}}} \int_{0.1\ \mathrm{MeV}}^{\infty} \sigma_f(^{238}\mathrm{U})\, \phi_f(r, E, t)\, \mathrm{d}E\, \mathrm{d}A \qquad (4)$$

where S_{det} is the detector surface area, ϕ_f is the fission neutron flux entering the detector from fission in the spent fuel element (SFE), and σ_f (^{238}U) is the ^{238}U fission cross-section. Here we calculate the detection sensitivity or response (relative counting rate) of the 20 threshold detectors (^{238}U) to fissions taking place in each of the 25 SFE cells.

Tables 3–6 show the detection sensitivity at the 20 surrounding threshold detectors for fission taking place in a corner fuel cell (cell number 1), cell number 3, cell number 7 and the center fuel cell (cell number 13). A total of 100,000 neutron histories was used for each detector response calculation. The upper number in each table is the detector number (see Fig. 2), the middle number is the response of the detector to fission in the fuel cell (1, 3, 7 or 13), and the bottom number is the 1σ statistical error from the Monte Carlo calculation. In Table 3, for example, the highest detector response is for detectors 15 and 16, while the minimum response is for detectors 5 and 6. According to Fig. 2, fissions in cell 1 should yield the greatest signal in detectors 15 and 16 and the smallest signal in detectors 5 and 6; this is what is observed in

Table 3
Normalized fission neutron contribution ($\times 10^{-5}$ 1/cm^{-2}) from fuel cell number 1 to the 20 surrounding ^{238}U detectors ($m = 1, \cdots, 20$)[a]

1	2	3	4	5
1.5561	1.3000	1.3188	1.1166	0.6249
(0.121)	(0.100)	(0.116)	(0.123)	(0.131)
6	7	8	9	10
0.6169	1.0042	1.1637	1.3337	1.4429
(0.137)	(0.193)	(0.117)	(0.106)	(0.089)
11	12	13	14	15
2.2421	3.5954	5.5217	12.102	12.342
(0.099)	(0.072)	(0.050)	(0.039)	(0.038)
16	17	18	19	20
12.821	11.299	6.9161	3.5626	2.3326
(0.037)	(0.038)	(0.055)	(0.075)	(0.104)

[a]The number in parentheses is the relative error.

Table 4
Normalized fission neutron contribution ($\times 0^{-5}$ 1/cm^{-2}) from fuel cell number 3 to the 20 surrounding detectors[a]

1	2	3	4	5
0.9585	1.3283	1.2016	1.2755	0.8998
(0.108)	(0.123)	(0.127)	(0.107)	(0.110)
6	7	8	9	10
1.3217	1.5851	2.8479	2.9778	3.9652
(0.132)	(0.087)	(0.085)	(0.067)	(0.074)
11	12	13	14	15
4.9356	8.5606	13.298	8.9632	5.3120
(0.063)	(0.044)	(0.037)	(0.046)	(0.056)
16	17	18	19	20
3.6879	3.5105	2.6653	2.0600	1.2557
(0.066)	(0.083)	(0.079)	(0.102)	(0.138)

[a]The number in parentheses is the relative error.

Table 5
Normalized fission neutron contribution ($\times 10^{-5}$ 1/cm^{-2}) from fuel cell number 7 to the 20 surrounding detectors[a]

1	2	3	4	5
1.7172	2.3321	1.7330	1.5961	0.9105
(0.095)	(0.103)	(0.079)	(0.103)	(0.114)
6	7	8	9	10
1.2663	1.6608	2.0034	2.3594	2.0501
(0.124)	(0.108)	(0.123)	(0.097)	(0.082)
11	12	13	14	15
2.3004	3.6301	5.8615	5.9936	4.5161
(0.090)	(0.063)	(0.059)	(0.053)	(0.056)
16	17	18	19	20
5.1384	6.4775	5.5769	3.2352	2.2710
(0.059)	(0.049)	(0.057)	(0.063)	(0.095)

[a]The number in parentheses is the relative error.

Table 6
Normalized fission neutron contribution ($\times 10^{-5}$ 1/cm^{-2}) from fuel cell number 13 to the 20 surrounding detectors[a]

1	2	3	4	5
2.0052	2.5638	3.3976	2.8412	2.0949
(0.089)	(0.083)	(0.068)	(0.069)	(0.103)
6	7	8	9	10
2.3463	3.0842	3.6603	3.2007	1.8752
(0.094)	(0.092)	(0.115)	(0.086)	(0.077)
11	12	13	14	15
2.1587	2.9600	3.4337	2.7217	2.0969
(0.096)	(0.062)	(0.091)	(0.068)	(0.090)
16	17	18	19	20
2.2889	3.0018	3.2570	2.9003	1.9531
(0.103)	(0.081)	(0.083)	(0.074)	(0.091)

[a]The number in parentheses is the relative error.

Table 3. Similar effects are seen in other detectors symmetrically located about SFE cell 1. For fission in cell 3, Table 4 shows that detector 13, which is closest to cell 3, has the highest response while detectors 1 and 5, which are furthest away, have the lowest response.

After several collisions of a source neutron with lead, the slowing down time of an average energy neutron from the source spectrum is derived by

$$\bar{t} = \frac{\int_0^\infty t N_s(E,t)\,dt}{\int_0^\infty N_s(E,t)\,dt} \tag{5}$$

where $N_s(E,t)$ is the number density of interrogation neutrons at energy E at time t. By integration, the relationship between the neutron mean energy and the slowing down time in neutron spectrum is obtained as

$$\bar{E} = k/(\bar{t} + t_0)^2, \tag{6}$$

where k and t_0 are only dependent variables of the slowing down medium; k is 1.67×10^5 eV μs and t_0 is 0.8665 μs for the fuel assembly in the designed lead spectrometer.

The energy resolution in the spent fuel is very important. The presence of spent fuel, which contains light (compared to lead) nuclei like oxygen and zirconium, not only broadens the energy resolution but also distorts the energy distribution resulting from the characteristics of the fission fragments, fertile and fission materials. Around the average energy, the energy resolution of the distribution at the slowing down time was fitted to the form

$$\phi(E) = AE^{1/2} \exp[-B(E-\bar{E})^2/(\bar{E}R)^2] \tag{7}$$

where A is a normalization factor, B is a constant, $\bar{E}$ is the mean energy and R is the energy resolution of the spectrum. The energy resolution ($(\Delta E/E)_{FWHM}$) in the SFE was 0.3–0.9 in the assay energy range, corresponding to 12–1291 μs slowing down time [5]; this resolution is sufficient for fissile assay. The intense neutron flux and adequate resolution of the LSDTS provide an active interrogation assay system which has a linear response from the sub-threshold neutron region to the resolved resonance region.

2.2. Modeling of neutron emission tomography

Neutron emission tomography (NET) is an effective and valuable method to study the internal fissile material distribution inside of spent fuel which is important for spent fuel management, utilization and safeguards [11,12]. The prompt fission neutron detection method is the only direct way to analyze the fissile materials in the spent fuel assembly. The 15×15 spent fuel rods in a PWR assembly were rearranged to make an equivalent homogenized 5×5 cell configuration (see Figs. 1 and 2). Each cell is 2.52 cm on a side and it is assumed that there is no variation of burnup distribution along the axial direction in each fuel cell. Thus, the variation is constrained to just the radial direction. This assumption is made here to simplify the demonstration of this technique. An axial scan of the spent fuel assembly can also be performed to obtain fuel distributions in "slices" along the axis. The induced fission neutrons from the fissile isotopes are detected by the surrounding 20 threshold detectors (^{238}U) which have a $3.94 \times 30\,cm^2$ surface area as shown in Fig. 2. The model of NET is based on the fact that all induced fission neutrons caused by interrogation neutrons in each fuel cell contribute to detection in the surrounding 20 detectors over the assay energy interval (1 keV to 0.1 eV). The simple form for counts in a detector is given by

$$D_{m,c,E} = QR_{m,c}[(MN)_{U235} + (MN)_{Pu239} + (MN)_{Pu241}]_{c,E} \tag{8}$$

where $D_{m,c,E}$ is the response of detector m to fission in cell c at the slowing down time corresponding to interrogation neutrons of energy E causing the fission. Q is a constant of proportionality which is a function of detector mass, position and size and the neutron source strength. $R_{m,c}$ is the relative counts in detector m per fission neutron in cell c and N_i is the number density of each fissile isotope i. M_i is the time-averaged fission neutrons ($\overline{\nu\sigma_f\phi}$) for fissile isotope i, that is the number of fission neutrons in cell c from fissile isotope i over a slowing down time interval Δt per source neutron, as given by

$$\frac{\int_{\Delta t} \nu\sigma_f\phi\,dt}{\int_{\Delta t} dt}. \tag{9}$$

Finally, the fission neutron contribution to a detector is summed over all cells to give a total detection signal

$$D_{m,E} = Q \sum_{c=1}^{25} R_{m,c}[(MN)_{U235} + (MN)_{Pu239} + (MN)_{Pu241}]_{c,E}. \quad (10)$$

The $R_{m,c}$ was created by the MCNP transport code between detectors and fuel cells with the assumption that the relative reference response R had noiseless data (equivalent to a very large number of detector counts). Additionally, there was a known relationship between mass projection elements and detector signals.

The assay system is generally expressed in matrix form as

$$\begin{bmatrix} D_1 \\ D_2 \\ \vdots \\ D_m \\ \vdots \\ D_{20} \end{bmatrix} = Q \cdot \begin{bmatrix} R_{1,1} & R_{1,2} & \cdots & R_{1,25} \\ \vdots & & & \\ & R_{m,c} & & \\ \vdots & & & \\ R_{20,1} & & \cdots & R_{20,25} \end{bmatrix} \cdot \begin{bmatrix} N_{U235,1} & M_{U235,1,E} + N_{Pu239,1} & M_{Pu239,1,E} + N_{Pu241,1} & M_{Pu241,1,E} \\ \vdots & & & \\ N_{U235,c} & M_{U235,c,E} + N_{Pu239,c} & M_{Pu239,c,E} + N_{Pu241,c} & M_{Pu241,c,E} \\ \vdots & & & \\ N_{U235,25} & M_{U235,25,E} + N_{Pu239,25} & M_{Pu239,25,E} + N_{Pu241,25} & M_{Pu241,25,E} \end{bmatrix}$$

$$\bar{D} = Q \cdot \bar{R} \cdot \overline{MN}. \quad (11)$$

Eq. (11) is solved iteratively using the methods of Refs. [12–15].

2.3. Spatial sensitivity of fissile assay

The sensitivity calculations were examined with the use of the MCNP code to determine to what extent a cross-section representing an array of void (partially or totally missing rods) and intact spent fuel cells could be reconstructed. Studies were made on how sensitive the reconstruction is to detect diversion, the existence of burnup gradients close to control rods and the spatial relative burnup distribution of fissile nuclei. Therefore, by the reconstruction [12–15] of fuel cell density, we could find the fuel cell location and the total fissile mass in the cell when fuel rods were missing in the location and replaced by depleted or dummy fuel rods.

The spatial distribution of all of the fissile materials and the total mass consistency were investigated by reconstruction in the fuel assembly. The 20 surrounding threshold detectors detected the fission neutrons emanating from inside the fuel assembly. We could look at what happens inside by removal or replacement of fuel cells (partially or totally), increasing cell density or making gradient cell densities. Single cell removal (void) was first considered at typically selected cell numbers 1, 3, 7, or 13 by considering the symmetry coupling of inside fuel cells to detectors; grouping removal was also investigated at cell numbers (1, 2, 6, 7) and (7, 8, 12, 13) to see the reconstruction sensitivity.

Figs. 3 through 6 show the sensitivity for finding the missing cell location and determining cell density at the selected single cell void. Since the detector counts are assumed to be noiseless, the fluctuations are primarily the result of the Monte Carlo statistical errors in determining the elements of the detector response matrix $\bar{R}$ (see Eq. 11). Figs. 7 and 8 also represent the grouping of four

missing cells and give reasonably reconstructed cell values even though there are slightly fluctuated cell values in reconstruction. Additionally, partially voided cell cases are reconstructed as a replacement of depleted fuel cells in the assembly. Cell number 1 is replaced by the cell which has 0.2 in density (Fig. 9) and cells 3 and 7 are 0.4 in density (Figs. 10 and 11, respectively). Figs. 9–11 show the partially voided cells in good agreement, even though there was a fluctuation of inside cell densities in reconstruction.

However, in the reconstruction of partially or totally voided cell cases, the determination of the density of the center cell (cell number 13) was less accurate than that for the other cells. In addition when the void part moved into the center cell, a general smeared decrease in the mass of cells neighboring the missing cell occurred. For a single missing cell case located at the outer zone of the assembly, the reconstruction of the void cell showed almost 97% accuracy in determining the

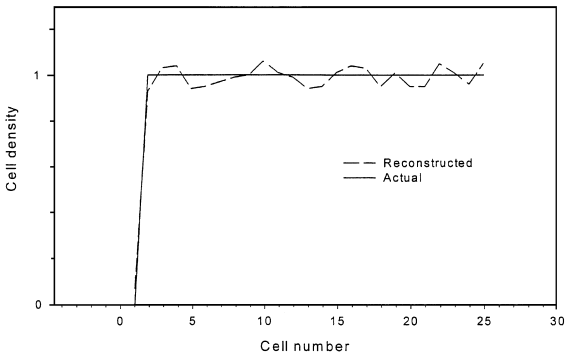

Fig. 3. Reconstruction of 25 fuel cells: cell number 1 is void (unit density is that for the homogenized PWR fuel element).

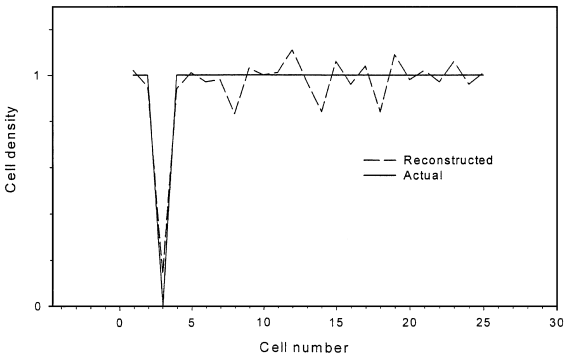

Fig. 4. Reconstruction of 25 fuel cells: cell number 3 is void (unit density is that for the homogenized PWR fuel element).

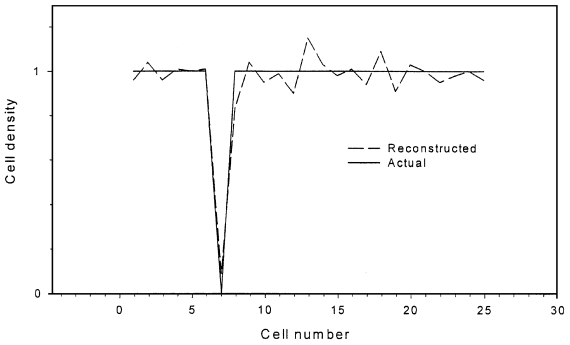

Fig. 5. Reconstruction of 25 fuel cells: cell number 7 is void (unit density is that for the homogenized PWR fuel element).

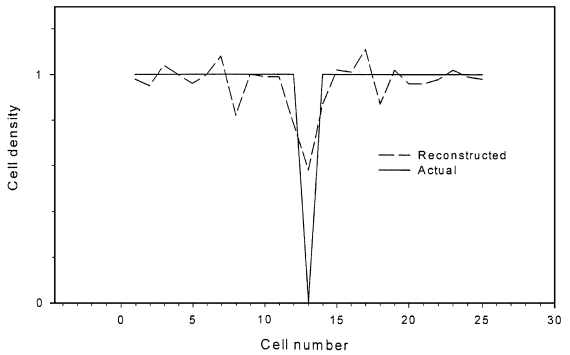

Fig. 6. Reconstruction of 25 fuel cells: cell number 13 is void (unit density is that for the homogenized PWR fuel element).

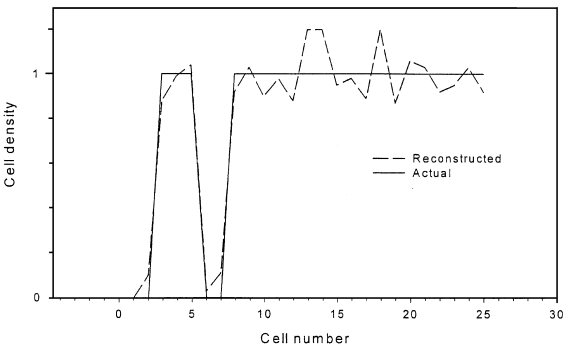

Fig. 7. Reconstruction of 25 fuel cells for the grouping removal of cells: cell number 1, 2, 6, 7 are void (unit density is that for the homogenized PWR fuel element).

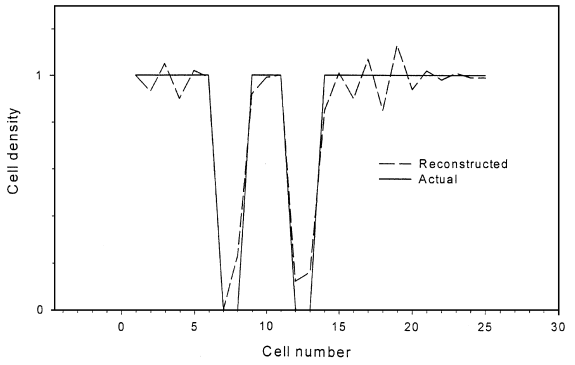

Fig. 8. Reconstruction of 25 fuel cells for the grouping removal of cells: cell number 7, 8, 12, 13 are void (unit density is that for the homogenized PWR fuel element).

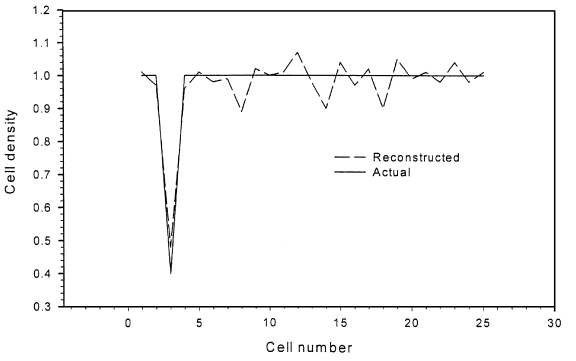

Fig. 10. Reconstruction of 25 fuel cells for partially voided cells: density of cell number 3 is 0.4 (unit density is that for the homogenized PWR fuel element).

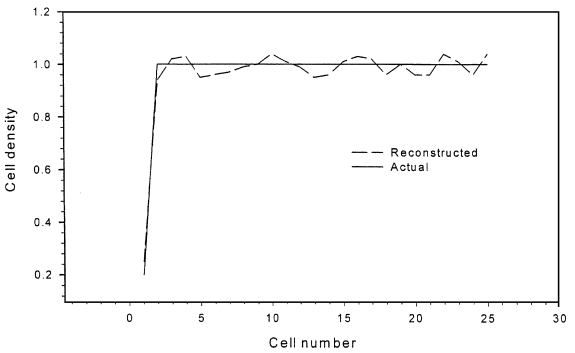

Fig. 9. Reconstruction of 25 fuel cells for partially voided cells: density of cell number 1 is 0.2 (unit density is that for the homogenized PWR fuel element).

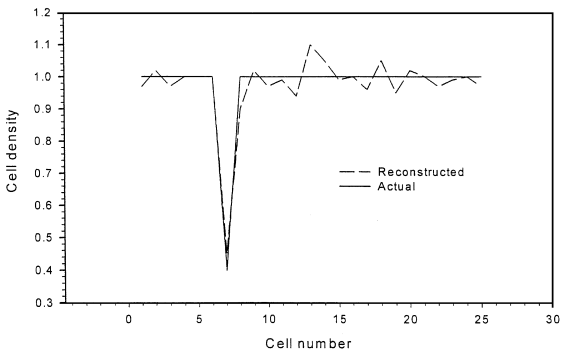

Fig. 11. Reconstruction of 25 fuel cells for partially voided cells: density of cell number 7 is 0.4 (unit density is that for the homogenized PWR fuel element).

simulation cell density, compared to $\sim 60\%$ for a missing center cell case. However, a grouping void accuracy of $\sim 93\%$ sensitivity was obtained even for a center zone removal. Therefore, when the more voided cells are clustered along a given projection element, reconstruction gives an increased accuracy, even near the center area of an assembly.

When the fuel assembly is located beside a control rod, the burnup gradient is created inside the fissile materials because of the different spatial neutron flux. Fig. 12 shows the reconstruction when there is a gradient of cell densities. Reconstruction still gives good agreement even though there is some depression in the center zone cell densities.

Another tomographical application using LSDTS was the determination of diversion sensitivity. Simply, the diversion sensitivity is defined as the ratio of the percent change of fuel cell density corresponding to a percent change of the total mass in the fuel cell. In this diversion sensitivity calculation, a certain ratio of fissile mass which is extracted in the typically selected cell is added to surrounding cells; this was done to keep the total fissile mass constant. In Fig. 13 cell number 1 was voided and 1/3 of the mass of cell number 1 was added to the surrounding 2, 6, and 7 cells, thus keeping total mass constant. In Fig. 14 cell number 2 was voided and 0.2 of its mass was added to

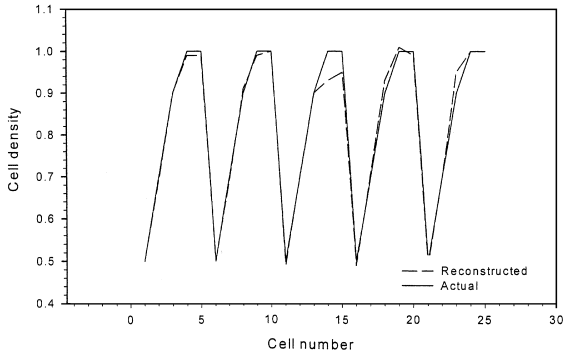

Fig. 12. Reconstruction of 25 fuel cells when burnup gradients exist near the control rods: gradients are 0.5, 0.7, 0.9, 1.0 far away from the control rods.

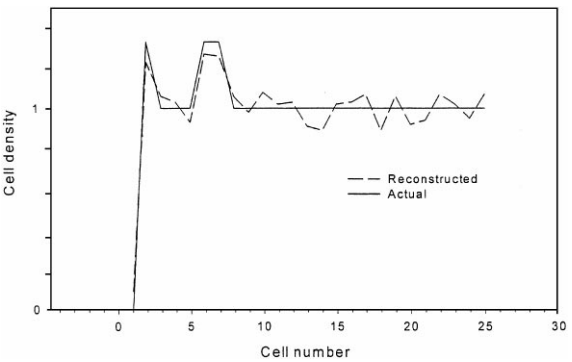

Fig. 13. Reconstruction of 25 fuel cells in diversion sensitivity: cell number 1 is extracted and same density ratio (0.333) is

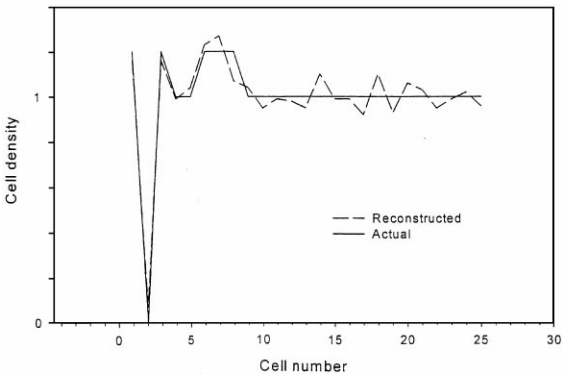

Fig. 14. Reconstruction of 25 fuel cells in diversion sensitivity: cell number 2 is extracted and the same ratio (0.2) is added in surrounding cells (1, 3, 6, 7, 8) (unit density is that for the homogenized PWR fuel element).

Table 7
Comparison of the consistency of the total assembly fissile mass in cell void cases (MCNP code was used to get the surrounding threshold detector counts)

Condition	By reconstruction (%error)	By sum of all surrounding detector signals (%error)
Cell number 1 void	0.041	0.0811
Cell number 3 void	0.032	0.186
Cell number 7 void	0.08	0.425
Cell number 13 void	4.26	0.83
Grouping void (1,2,6,7)	0.781	0.825
Grouping void (7,8,12,13)	0.751	2.51

surrounding cells 1, 3, 6, 7, and 8. Figs. 13 and 14 show the diversion sensitivity at cell numbers 1 and 2 in good agreement. As shown in Figs. 13 and 14, even though there are fluctuations of reconstructed cell densities, the total fissile mass of fuel assembly determined reasonably well.

There is also a comparison of the total assembly fissile mass consistency by the tomographical approach and by the sum of all surrounding detector signals. Table 7 shows the comparison of the total assembly fissile mass consistency at cell void cases with the assumption of noiseless detection data. The result shows quite well the total assembly fissile mass in single and grouped voids. However, the center cell void has a greater influence on the accuracy of the reconstruction method. Therefore, our new approach works fine as a result of the sensitivities of the spatial fissile assay and the assembly fissile mass consistency for very low statistical error in the detector counts.

3. Effects of detector counting statistics for a working system

Several sensitivity calculations were examined under the assumption of perfect (noiseless) detector counts. However, in an actual experimental

Table 8
Comparison of the assembly fissile mass consistency by detector count fluctuations under the assumption of a Poisson distribution (MCNP code was used to get the surrounding threshold detector counts)

Relative detector counts fluctuation (%)	By reconstruction (% error) Cell 1 void
0.00	0.041
0.05	0.261
0.10	0.656
0.20	1.160
0.50	2.999
0.70	1.404
1.00	4.464

measurement, there are detection fluctuations. Therefore, the detection error limit was examined using MCNP under the assumption of a Poisson distribution of detector counts for the tomographical application to analyze the assembly total fissile mass in the designed LSDTS. For noiseless detector data, the tomographical result shows excellent reconstruction in several sensitivity calculations. However, increasing the fluctuation of detector counts, like in actual experiments, gives a worse reconstruction.

Detector counts were created with the help of random number generation by the assumption of the Poisson distribution with fluctuations around the mean value of a given percent rate of fluctuation. Table 8 shows the comparison of the assembly total fissile mass consistency at the cell number 1 void case by increasing the fluctuation of the detector counts. From the table, the results show that the accuracy of the total mass determination decreases with increasing detector fluctuations, i.e. with poorer counting statistics. This points to the need for good counting statistics in these types of measurements which can be obtained through more efficient detectors, increased neutron source intensity and longer counting times.

4. Discussion of results

The LSDTS can be used to assay the spatial distribution of total fissile materials by detecting the prompt fast fission neutrons from a spent fuel assembly, using properly selected energy interrogation neutrons. The reconstructed tomographic results showed that the total fissile mass in a fuel cell was located effectively at the right place as a component of the assembly and information on fuel burnup distribution as well as rod diversion could be obtained. The partially or totally void fuel cell was evident, as was the structure of the fuel cells, although the density was not correct and the neighboring cells densities were smeared out; however, the sum of the reconstructed total fissile mass in all fuel cells was consistent with the SFE fissile mass. Specially, in several sensitivity calculations, reconstruction showed the expected spatial fissile mass distribution with some fluctuations.

From simulating the actual detector measurements, less detection fluctuation is more favorable to the tomographical fissile assay and the sum of the surrounding detector counts gives more reliability in the assembly fissile mass consistency with detection fluctuation. As reported in Ref. [5], a small accelerator can provide quite high counting rates in the designed LSDTS and thus provide accurate tomographic results in a short period of time. The LSDTS system is a very sensitive device for analyzing the spatial distribution of total fissile materials in a spent fuel assembly and is shown by the sensitivity calculations to be successful for a practical and routine assay operation.

5. Conclusion

The LSDTS is applicable for a practical and effective spatial total fissile assay of spent fuel. The assay device can analyze the fissile mass tomographically at the correct fuel cell locations with counting statistics that can be obtained with a small accelerator [5]. The new tomographical approach to investigate the spatial distribution of the total fissile mass was successful in the designed LSDTS assay device. In addition to the radial assay of total fissile contents, the threshold detectors can be segmented axially to provide an axial sensitivity to detection of fissiles in the fuel; by scanning the spent fuel assembly information can be obtained on both axial and radial distribution of fissile contents. The LSDTS assay system

should be calibrated with fuel of various known composition for practical and precise assay.

Finally, an optimized assay device could be applicable to any type of spent fuel in the proper assay energy range, even in the broadened energy resolution of the system caused by the presence of the spent fuel. LSDTS is also applicable to the detection of internal fuel density variations in sintered fuel rods for the safe and effective advanced fuel development and for nuclear waste assay and management.

References

[1] A. DeVolpi, E.A. Rhodes, Mat. Eval. 40 (1982) 1273–1279.
[2] L.W. Person, A.E. Klickman, E. Rhodes, Trans. Am. Nucl. Soc. 28 (1987) 127.
[3] B.D. Sawicka, Nucl. Instr. and Meth. A 299 (1990) 468.
[4] N.M. Abdurrahman, R.C. Block, D.R. Harris, R.E. Slovacek, Y.-D. Lee, F. Rodriguez-Vera, Nucl. Sci. and Eng. 115 (1993) 279.
[5] Y.-D. Lee, N. Abdurrahman, R.C. Block, D.R. Harris, R.E. Slovacek, Nucl. Sci. Eng. 131 (1999) 45.
[6] C.D. Bowman, Nucl. Sci. Eng. 75 (1980) 12.
[7] O.K. Harling, Nucl. Instr. and Meth. A 119 (1974) 217.
[8] H.G. Ebert, Proceedings of The Third Conference on Accelerator Targets Designed For The Production of Neutrons, Belgium, September 18–19, 1967.
[9] J.F. Briesmeister. MCNP : a general Monte Carlo code for neutron and photon transport, Technical Report LA-7396-M, Los Alamos National Laboratory, September, 1986.
[10] A.G. Croff, ORIGEN2 – a Revised and updated version of the Oak Ridge isotope generation and depletion code, ORNL-5621, ORNL, 1980.
[11] Y.-D. Lee, Appl. Radiat. Isot. 48 (10–12) (1997) 1535.
[12] Y.-D. Lee, Proc. of the Korean Assoc. Radiat. Prot. (1997) 131.
[13] Y. Censor, P.P.B. Eggermont, D. Gordon, Numer. Math. 41 (1983) 81.
[14] Y. Censor, G.T. Herman, Row generation methods for feasibility and optimization problems involving sparse matrics and their applications, in: I.S. Duff, G.W. Stewart (Eds.), Sparse Matrix Proceedings-1978, Society for Industrial and Applied Mathematics, Philadelphia, (1979), pp. 197–219.
[15] G.T. Herman, A. Lent, Comput. Biol. Med. 6 (1976) 273.